sciendo

POLISH MARITIME RESEARCH 4 (100) 2018 Vol. 25; pp. 73-82
10.2478/pomr-2018-0134

SIMPLE COMPUTATIONAL METHODS IN PREDICTING LIMIT LOAD OF HIGH-STRENGTH COLD-FORMED SECTIONS DUE TO LOCAL BUCKLING: A CASE STUDY

Paweł Bielski
Leszek Samson
Gdansk University of Technology,Faculty of Ocean Engineering and Ship Technology, Poland
Oskar Wysocki
Jacek Czyżewicz
Gdansk University of Technology, Faculty of Mechanical Engineering, Poland

ABSTRACT

Cold-formed thin-walled sections are prone to local buckling caused by residual stresses, geometrical imperfections and inconsistency of material properties. We present a real case of buckling failure and conduct a numerical and experimental study aimed to identify methods capable of predicting such failures. It is important because designers of structures are getting more FEA-oriented and tend to avoid lengthy procedures of cold-formed structures design. Currently adopted methods are complicated and require patience and caution from a designer which is reasonable in case of the most important structural members but not necessarily so in ordinary design. Since it is important, we offer an insight into several FEA and manual methods which were sufficient to predict the failure while remaining fairly simple. Using a non-uniform partial safety factor was still necessary. We hope that this paper will be of interest for people performing a lot of routine analyses and worrying about reliability of their computations.

Keywords: high-strength steel structures; cold-formed thin-walled sections; local buckling; stability of structures; Eurocode 3 safety factor

INTRODUCTION

The paper addresses the problem of local stability of cold-formed high-strength steel members in the context of industrial design. We examined a real case of buckling failure and performed several relatively effortless computational steps which would have been enough to predict and prevent this failure. It is an important issue, since most currently available procedures are either complicated or demand non-obvious informations on residual stresses, field of imperfections, changes in ductility, etc. Cold-formed steel members are equally popular in coastal and offshore engineering (eg. [9]), machine industry, civil engineering and any branch of industry relying on steel structures. With the growing popularity of FEA software in average design offices, the design practices are shifting more towards numerical analysies of individual cases. As long as no extraordinary structural members of great importance are concerned, it is easier and faster to perform simple FEM calculations than to apply complicated procedures. Of course, if complicated structures requiring special care are involved or a specialised research study is executed, geometrical imperfections are measured or assumed in order to get more correct results (eg. 19]). In contrast, performing such precise computations in regular design practice is considered too costly. As a result, according to our own experience and observations, local stability is often overlooked or overly simplified in the design phase, since the available methods are beyond the reach of

an average engineer or are too time-consuming. What is needed is a feasible method for quick and reliable calculation of ultimate load of such structures. Since it is important, we try to identify the main neglections on the stage of design which led to this particular failure. In the same time we try to suggest some alternative methods which might be sufficient while remaining relatively simple and straightforward to execute by any structural engineer.

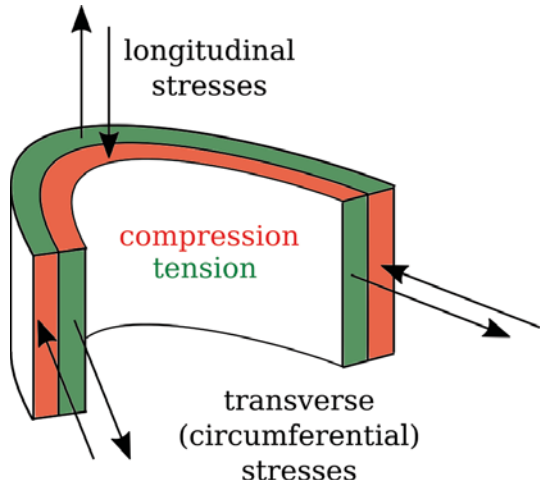

Fig. 1. Simplified visualisation of the final residual stresses in a corner after the "spring-back" phase of cold-forming according to Quach [11]; note that in reality the stress distribution especially in the trasnverse direction is considerably more complex than in the figure

Although many recommendations for calculating the cold-formed sections load capacity already exist (notably AISI [3] and Eurocode 3 [5]), a universal and simple method of safe design is yet to be developed. In 1975 Ingvarsson came up with a theoretical analysis which proved the existence of residual stresses not only in the circumferential direction of a profile (perpendicular to the bending axis), but also in the longitudinal direction [6]. Magnitude of this stress component varies depending on the cold-forming conditions. This finding was of much importance for understanding the cold-formed section strength, since longitudinal stresses directly affect the overall bending load capacity. In 1981 Crisfield developed a numerical method allowing to compute non-monotonous equilibrium paths and thus enabled to predict post-buckling behaviour [4]. In 1990 Weng and Pekoz exhibited that cold-forming induces a field of residual stresses which is different from that of hot-rolling, regardless of the fact that at the time AISI did not distinghish between these two technologies in terms of calculating the load capacity [18]. In the following years a series of numerical, analytical and empirical methods were developed to deal with the problem. Schafer and Pekoz insisted on including both residual stresses and imperfections as initial conditions in numerical modelling and proposed to employ at least 2 different states of geometrical imperfection based on eigenmodes along with flexural residual stresses in all elements [13]. Since residual stresses in the cold-formed corners can reach even up to 50% of the initial yield stress, membrane stresses should also be assumed in corner areas of such models. The same authors popularised usage of the Direct Strength Method in engineering practice as an alternative to the commonly acknowledged Effective Width Method [3] due to the excessive complexity of the latter [14]. Yu and Schafer executed some experimental studies on local buckling behaviour of cold-formed members [21] and discussed usability of cumulative distribution function in adopting the magnitude of initial imperfections [22]. Quach wrote a massive PhD dissertation on multiple aspects of modelling the development of the cold-forming stresses [11] and together with Qiu they exhibited that in the process of cold-forming not only residual stresses are established, but also modifications of the yield stress value are applied (generally increase of this value) and even more importantly the ductility of material is changed, which causes the corner cracking during local buckling [12]. Laim et al. compared empirical and numerical methods for predicting the cold-formed sections buckling behaviour and coupled the study with the experimental work on real specimens. Usability of Eurocode 3 methods was confirmed, however only medium strength (up to 460 MPa) steel was tested and still a need for "new design guidelines" was stated [7]. Abambres and Quach explicitly stated that "One of the most challenging aspects in FEA aimed to simulate the real behaviour of steel meber, is the modelling of residual stresses" [1]. Szymczak and Kujawa [15] and Lu [8] provided additional analytical solutions to predict the buckling behaviour of cold formed-members based on eigenmodes, however these methods are not always suitable to applications where a very local form of stability loss is expected (such as development of individual wrinkles [20]). Wang et al. conducted experimental and numerical tests again in terms of Eurocode 3 efficiency, however this time a high strength S700MC steel was involved. The standard procedure was found to be insufficient to assure safety of cold-formed structures, stating that the "Partial safety factor γ_{m0} greater than the currently adopted value of unity is required for high-strength steels" [17]. To date there is no reliable and fast method liberating a designer from identifying or assuming complex imperfection and stress fields in the process of cold-formed members design.

In the paper we present a real case of failure of a cold-formed high-strength steel member along with description of the overly simplified design methods which might have led to over-estimation of the structure load capacity. Later we describe a little more complex, however still relatively simple numerical methods (without introducing random or measured imperfection field, residual stresses or changes in material properties other than plasticity), which were used in the following investigation of the failure. Lastly we present a controlled destructive test carried out on another specimen of the discussed beam type and we conlcude on usability and safety of the executed computational methods in this particular case. Some conclusions regarding Eurocode 3 procedures are then drawn. It should be noted that the work featured in the paper is an extension and development of the study presented earlier at a conference [2].

MATERIALS AND METHODS

OBJECT OF THE STUDY

The discussed beams are strucutral members of a refuse collection vehicle more commonly known as garbage truck. Refuse Collection Vehicle (RCV) consists of a container body, a tailgate and a lifter. Its main function is collection, compaction and transportation of waste. The mechanism is powered by a hydraulic system supplied by the pump mounted on the truck's engine. A greater part of RCV is a welded steel structure designed to withstand a cyclic load produced by high pressure in hydraulic cylinders. Many of the load bearing elements are thin-walled structures, since mass reduction is an important factor of RCV development. Lighter vehicles can carry larger waste cargo due to legal limitations of total unit mass.

The examined beams were designed to resist the ejector plate during compaction of waste and discharging of the RCV. They were made of a high strength S700MC steel and consisted mainly of 3 to 5 mm thick steel sheets. The beams were manufactured using cold-forming (4 mm bending radius) and welding (backplate / reinforcing elements).

INITIAL FAILURE

We will use the term "beam A" to refer to the first failure. The beam was re-designed in the office as a part of mass reduction program. Originally only linear FEM calculations were performed in Autodesk Inventor and a generic, industry-ready solid geometry was used for this purpose. A screenshot of the analysis and its complex geometry is shown in Fig. 2. The structure was considered safe.

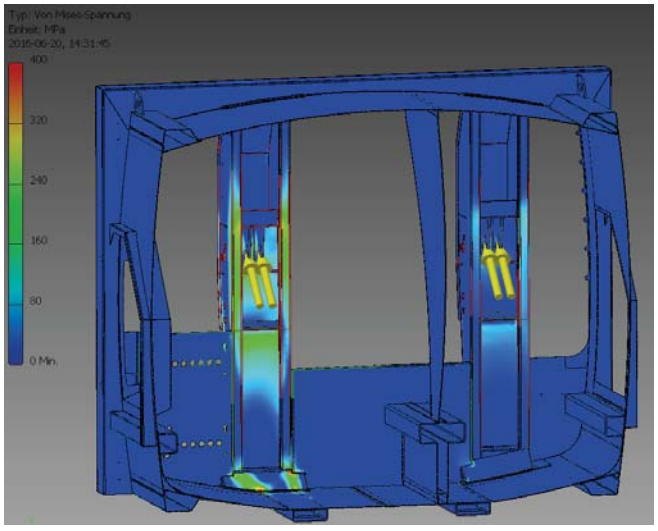

Fig. 2. Stresses obtained during the initial linear FEM calculations performed by designers beforehand; the stresses are evenly distributed along the beam length and generally do not exceed 400 MPa

What happened later was a buckling failure of the newly designed member during fatigue stress tests. The following investigation has been described in detail in the previous paper [2]. Here we will focus only on the essential part of the study.

According to the Eurocode 3 EN 1993-1-1 [5] recommendations, thin-walled steel sections can fall under one out of four categories. This classification is based on slenderness of the cross-section wall and describes section's local stability in plastic, elasto-plastic and elastic ranges. The class 1 and 2 sections are able to reach full plasticity without losing local stability. The class 3 sections are prone to buckling in an elasto-plastic state, after reaching yield stress partially but before entering plastic limit state. The class 4 sections lose stability in the elastic state, so full material strength can not be utilised (Fig. 3). The examined section was classified as a Class 3 element, which means that the elastic limit state should be reached before buckling.

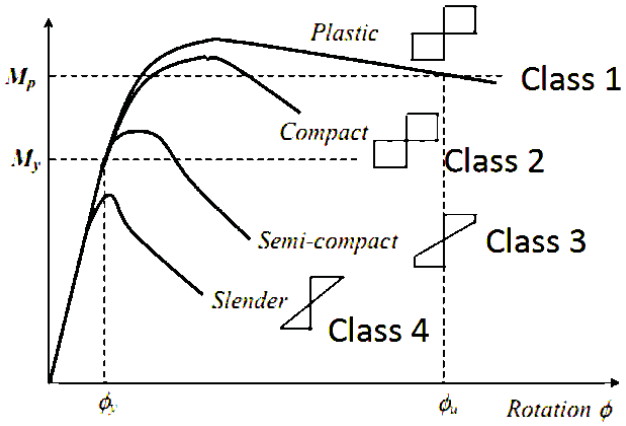

Fig. 3. M_y (elastic) and M_p (plastic) moment acting as an envelope for the real limit state moment for the Class 3 sections based on Eurocode 3 [5]

The rest of the study was conducted in Abaqus FEA software. The geometry was simplified and reduced to a mid-surface model (Fig. 4) with shell elements, since it is more appropriate for modelling bending of thin-walled structures and avoiding volumetric locking of solid elements [10]. Symmetry conditions were applied and several support conditions were assumed to create an envelope of possible solutions. It was later inspected in the following experimental work that the boundary conditions are actually simple pinned supports.

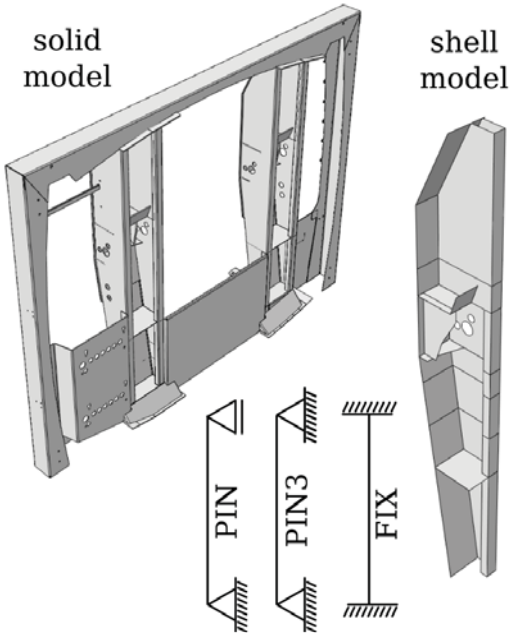

Fig. 4. Full geometrical model and its simplified representation as shell model with symmetry conditions and pinned / fixed support schemes

The real ultimate load was 280 kN and the one predicted by geometrical and material non-linear analysis was 320 kN, which equals about 15% of dangerous over-estimation. These results differ slightly from the ones obtained in the current study, because beams A and B had different spans (beam A 1880 mm, beam B 1780 mm) due to asymmetric layout of the RCV container body.

CONTROLLED FAILURE

An experimental study on beam B was conducted to further investigate the issue. The study was designed in a way to closely reflect the first case of failure. Simultaneous measurements of strains, load and displacement were performed. Preliminary measurements were executed to identify the real boundary conditions (supports) of the beam before destruction. As a result, we managed to reproduce the initial failure mechanism (deformation) while collecting additional information concerning what is happening within the structure.

Response of the system was recorded by means of strain and displacement measurements. Displacement was measured only in a single representative spot using a traditional dial distance indicator. This single displacement value was later used to identify the supports. Additionally, two cameras were used to record the experiment in two perpendicular directions. Strains were recorded using strain gauges placed in 10 different spots, however only 6 of them were active during destruction (limitations of the 6-channel recording device). The remaining gauges were used to identify stiffness of the supports. The spots were selected so that the following regions were covered:

- two boundary areas near the supports;
- a single representative cross-section without stiffeners, including areas of tension and compression;
- locations of the predicted local buckling, based on the observations from the initial failure and the coupled numerical study.

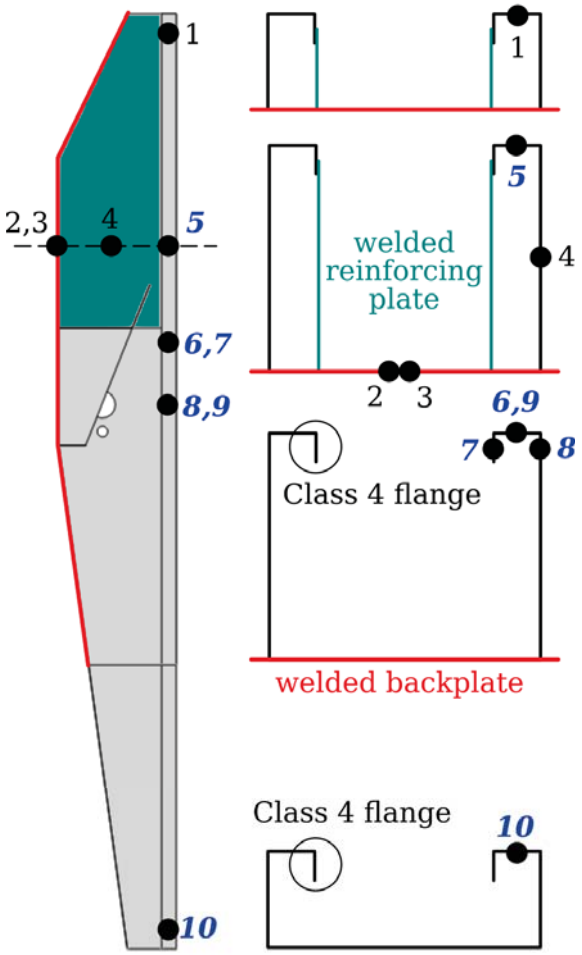

Fig. 5. Scheme of the examined beam with locations and numbers of strain gauges marked; the strain gauges active during the destructive test are indicated; note the differences in cross-section along the height of the beam

All of the strain gauges were oriented in a way to measure the longitudinal strains and not the circumferential strains. The equipment used to capture strains was composed of the following elements:

- bonded resistance strain gauges of 350 Ohm resistance and a gauge factor of 2.15;
- the strain gauge was arranged as a quarter Wheatstone bridge circuit;
- the bridge was connected via an instrumentation amplifier to one of the six 24-bit ADC channels;
- the converted signal from ADC was transferred to PC using a microcontroller;
- the *pySerial* Python library was used to register digital signals as text files;
- the data collected from the test was illustrated by Python scripts using *Numpy* package and *Matplotlib* plotting library.

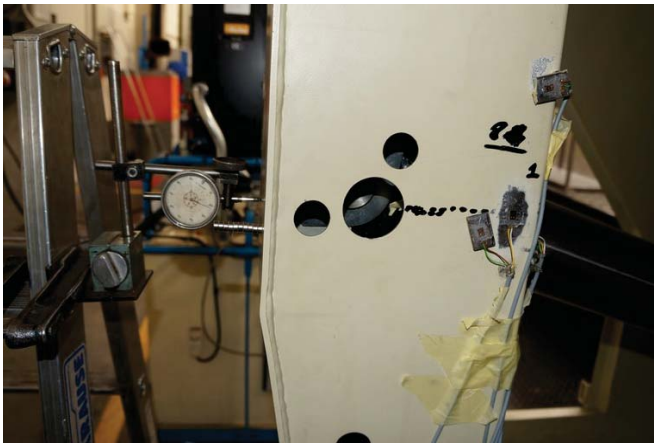

Fig. 6. Location of a dial distance indicator used to measure displacement; the same spot is used as reference displacement to compute ultimate load in the numerical analysis

The test stand varied slightly from the one used for the initial experiment. The load was applied by a 120 mm diameter cylinder at 15 degree angle relatively to horizontal direction. Maximum pressure of 270 bar (305 kN) was gradually achieved as a result of beam resistance to cylinder extension in approximately 1 mm/s. Inner resistance of the cylinder sealing was experimentally tested by means of repeated loading and taken into account in the final force calculation as 5 kN according to the hysteresis graphs. Measurement accuracy of pressure gauge was +-3 bar (3.5 kN).

Fig. 7. Location of the strain gauges on the real structure

Preliminary loading was conducted in a linear range to identify the stiffness of the beam. It was measured that the average displacement measured by the dial indicator is 1 mm per 37 kN of force, which corresponds to the simple support conditions assumed in the numerical model. Additionally, strain gauges 1 and 10 (boundary sections) and 2–5 (control sections) were used to measure strains, which were consistent with the simple support predictions (Fig. 10). Thus the boundary conditions provided by the frame were considered identified as near-zero rotational stiffness (Fig. 8)

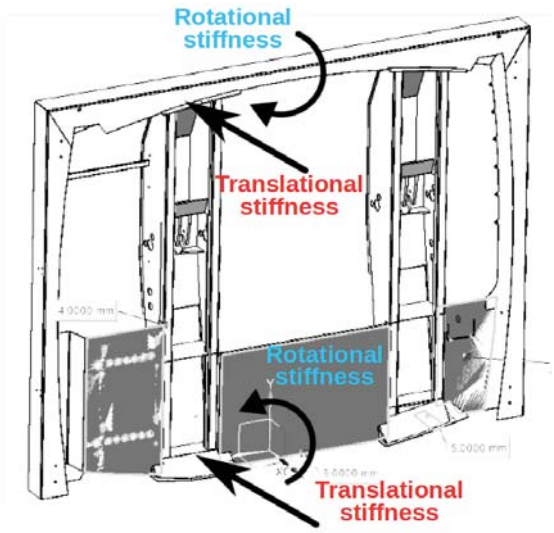

Fig. 8. Interpretation of the boundary conditions with regard to the stiffness of support provided by frame

After the initial failure several steel samples were cut from the original beam and from raw material as reference and tested for their mechanical properties (external analysis and expert opinion). The test focused on determining the chemical composition and tensile strength of specimens. It was confirmed that the steel used for production was actually S700MC in terms of chemical compounds. However, tensile tests exhibited reduced yield stress, averaging around 630 MPa for all samples. It was concluded that the reduced properties of the steel was faulty from the beginning. Nevertheless the 630 MPa value of yield stress was taken into consideration in the following numerical analyses. In general, three material variants were assumed: b700 (700 MPa yield with no hardening), b630 (630 MPa with no hardening), r700 (real strain-stress curve to examine the dangerous optimistic area near the yield stress shown in Fig. 9).

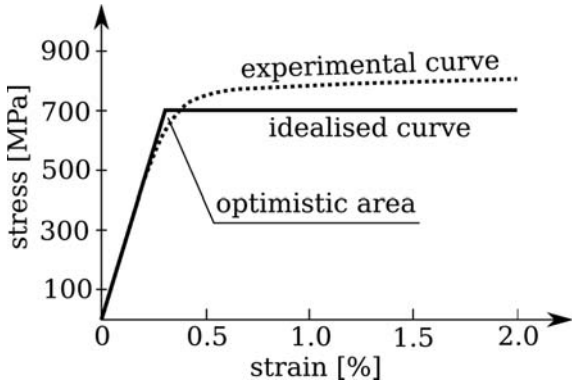

Fig. 9. Experimental (obtained by Winful et al. [16]) and idealised stress-strain relation of S700MC steel; note the optimistic area where the idealised curve delivers more stiffness than the experimental one

Numerical investigations covered LBA (linear buckling analysis), GMNA (geometric and material non-linear analysis) and linear static analysis. Imperfections were assumed basing on the LBA deformation and real deformation of beam A.

Manual calculations were perfomed too to provide an overview of possible results.

RESULTS

Results of the manual calculations performed on the simplified geometry are presented in Fig. 10. The elastic and plastic limit states form a boundary for the real ultimate load of a Class 3 section [5]. From these calculations we can conlcude that a failure should occur somewhere between the 330 kN and 478 kN values of concentrated force on a hydraulic cylinder. It is important to note that since the cross-sections vary between the loaded and control sections, the 0.46 ratio of maximum stresses were calculated taking both the different locations and sections into account.

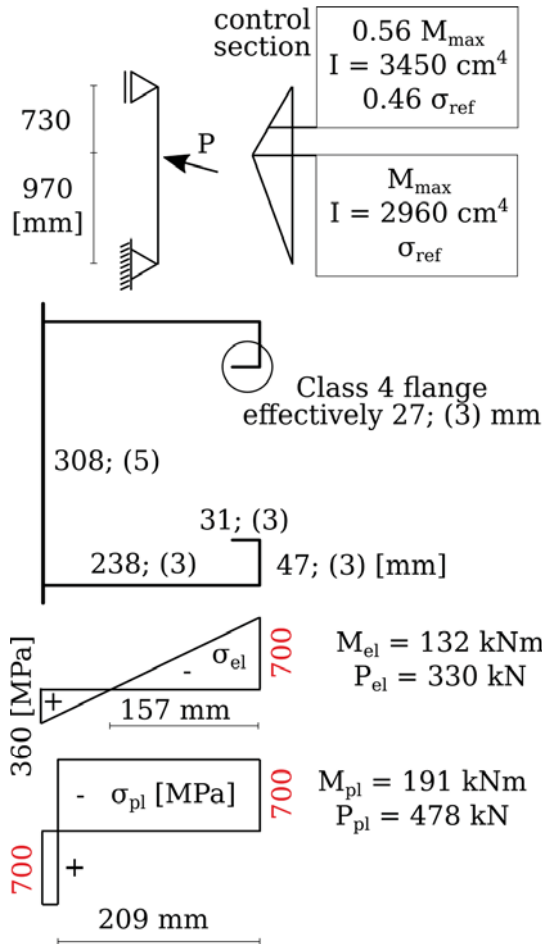

Fig. 10. Top: simplified diagram of the beam and its basic characteristic values; Bottom: Simplified cross-section of the beam ([length]; ([thickness]) of each element) and distribution of stresses in elastic and plastic limit states; M_{el} – extreme elastic moment, M_{pl} – extreme plastic moment, P_{el} and P_{pl} – forces corresponding to the moments

The post-buckling deformations of the A beam (initial failure) and B beam (controlled failure) are presented in Fig. 11. The large bulge on the side is located around the holes in both cases. This feature will be used to evalute the deformations obtained from the numerical analyses.

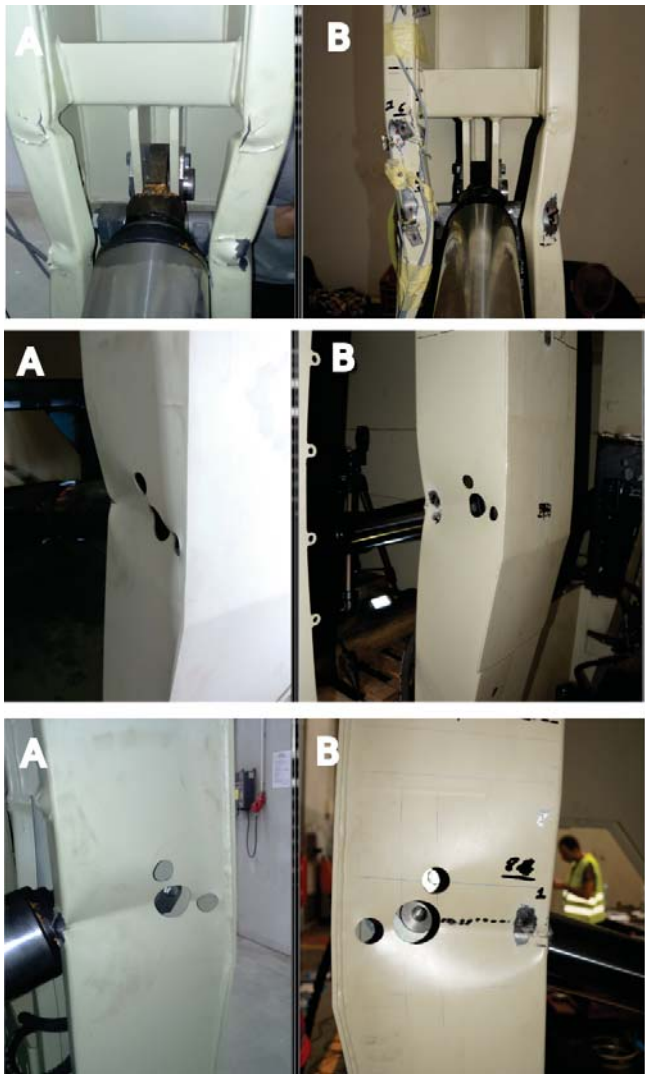

Fig. 11. Various views of the A (initial failure) and B (controlled failure) beams after buckling; the deformations are essentially the same

Results of the experimental loading are presented in Fig. 12 (direct values from strain gauges) and Fig. 13 (calcualted stresses). The first thing worth noting is the ratio of stresses between 5 (control section) and 6+9 (loaded sections) strain gauges, which equals the predicted 0.46 and justifies the boundary conditions assumed in the numerical model. The next thing are the strain gauges 7 curves, which indicate the largest values of stress and strain in the whole structure. The stresses are actually elevated in this location due to stress concentration, which was also exhibited in a simple linear numerical analysis (Fig. 14) The last thing to notice in the graph is development of the small bulge (Fig. 15) around the 220 kN force in the strain gauge 7 area.

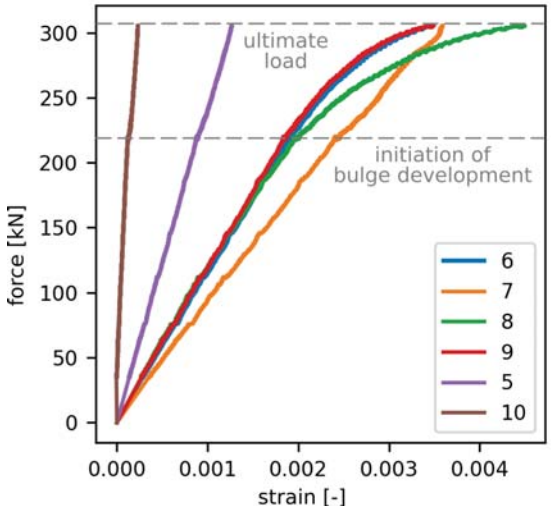

Fig. 12. Experimental strain-force curves obtained directly from the strain gauges during the destructive test; strain gauge numbers in the legend

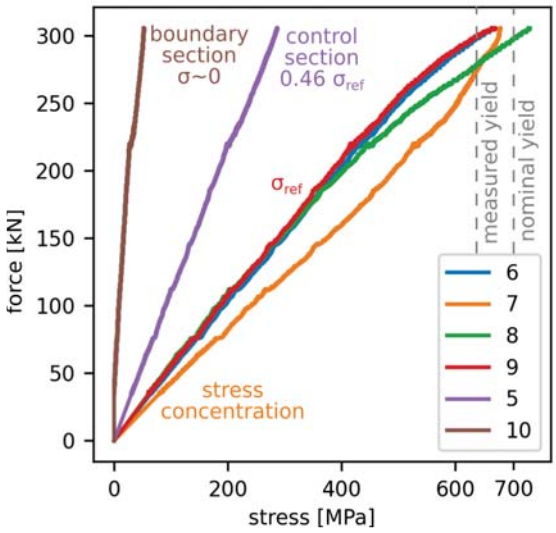

Fig. 13. Experimental stress-force curves computed from the strain curves using the strain-stress relationship by Winful et al. [16]

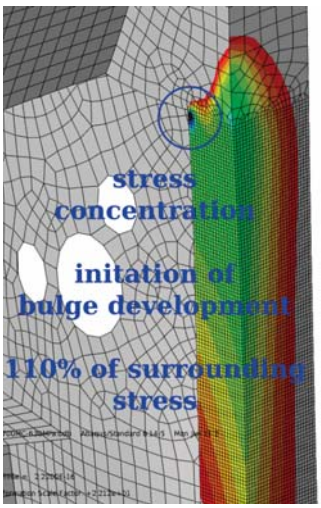

Fig. 14. Numerical representation of the local concentration of stresses around the strain gauge 7 area

Fig. 15. Deformation of the strain gauge 7 location due to local buckling; note the bulge developing straight at the center of the strain gauge

The first buckling mode obtained by means of LBA is presented in Fig. 16. The shape of deformation was always the same regardless of the type of imperfection applied, however the buckling factor varied accordingly. It was the highest (360 kN) for no imperfections and the lowest (325 kN) for both imperfections in the same time. Applying individual imperfections resulted in values lying between these two. Locations of the load imperfections were chosen basing on the shape of buckling mode.

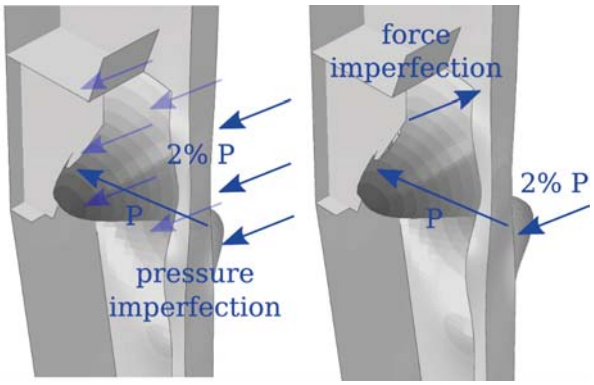

Fig. 16. The first buckling mode obtained via linear buckling analysis and the two types of imperfections applied during all analyses

Force-displacement equilibrium paths obtained from GNMA are presented in Fig. 17. Note that the curves are nearly linear up to the limit load, which means that no bulges are developed earlier. The 630 MPa with force imperfection and 630 MPa with pressure imperfection variants result in the same 322 kN limit load. However it is extremely important to notice that the post-buckling curves and deformations (Fig. 18) vary greatly and the one resulting from the pressure imperfection is far closer to the experimental one (Fig. 11) than the force imperfection variant.

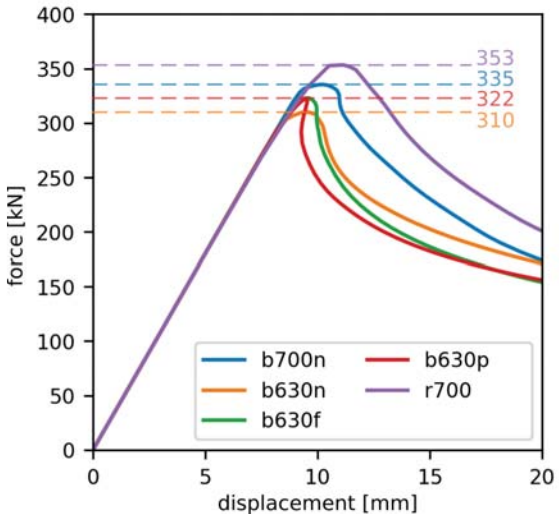

Fig. 17. Numerical displacement-force curves used to predict the ultimate load values; b – bilinear, r – real, 700 / 630 yield stress, n – no imperfection, f – force imperfection, p – pressure imperfection

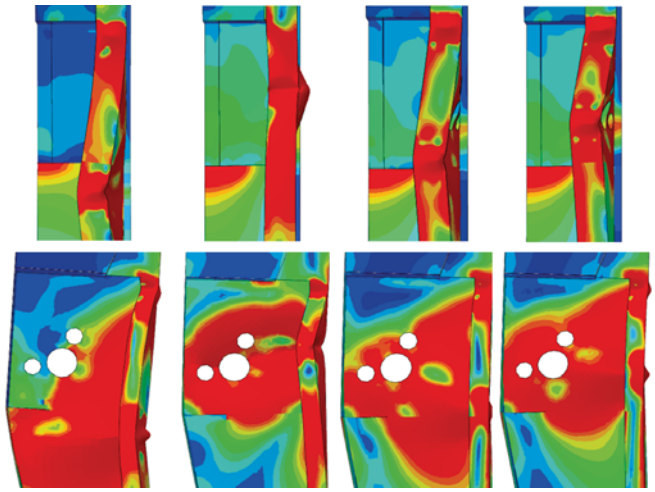

Fig. 18. Results of the numerical GNMA analyses, from left to righ: 700 MPa yield stress w/o imperfections, 630 w/o imperfections, 630 with force imperfection, 630 with pressure imperfection; note the different height of the lower bulge in each case

All of the numerical and manual results of limit load prediction are presented in Tab. 1 along with relative deviations from the experimental value.

Tab. 1. Ultimate loads obtained by various computational methods, the three LBA values stand for no imperfection, pressure imperfection and force imperfection; the two linear static values stand for the actual maximum moment section and the strain gauge 7 concentration region; the three GMNA values stand for 630 MPa with no imperfections, 630 MPa with load imperfections and 700 MPa with no imperfections

Source	Force [kN]	Difference [%]
Simplified plastic moment	478	56.7
Linear buckling analysis	360 / 344 / 338	18.0 / 12.8 / 10.8
Simplified elastic moment	330	8.2
Linear static analysis	315 / 362	3.3 / 18.7
Geometric and material non-linear analysis	310 / 322 / 335	1.6 / 5.6 / 9.8
Experimental measurements	305	0.0

DISCUSSION

All predicitions failed to meet the real value of the limit force, however they varied greatly among themselves. The manual calculations resulted in an envelope exceeding the real value by over 8% on the lower boundary, indicating that the Eurocode 3 predictions regarding the Class 3 section behaviour were not right in this case. The analysed beam had a non-uniform cross-section along its height and despite the fact that the weakest cross-section was taken under consideration, the real failure started in a different place–at the stress concentration region caused by the rapid cross-section change. This is an important observation which suggests that the Eurocode 3 regulations regarding thin-walled sections made of high-strength steel might not be always appropriate in case of partially reinforced members with changing cross-section.

All of the numerical equilibrium paths are nearly linear up to the limit load, while the experimental ones are slightly disturbed around the 220 kN mark due to the local buckling initiating around the strain gauge 7 area. This small bulge caused the overal stiffness of the whole beam to decrease, which can be deduced from the reduced slope angle of all curves over the 220 kN mark. This phenomenon is absent in the numerical analysis.

What happens with the strain gauge 7 location is essential for understanding the failure mechanism. From the very beginning the stresses and strains there are greater than in other parts of the structure, even though it is not a section of maximum bending moment. It is caused by the stress concentration in this region, which results in an early development of the out-of-plane bulge in this area. The same shape of deformation was achieved only in a load case with pressure imperfection and reduced 630 MPa yield stress (the last one in Fig. 18). Even though the GMNA limit load is not the lowest in this case (322 kN in contrast to 310 kN with no imperfections), the actual behaviour of a real structure was captured. It was not achieved in any 700 MPa yield stress variants with imperfections (not shown in the figures)–in each of these cases the lower bulge developed way too low. It implies that lowering the plastic yield stress by a safety factor might be more appropriate than lowering the overall limit load, since it may partially compensate for not involving residual stresses in the computations.

CONCLUSIONS

- Existing methods of analytical/empirical calculation or computer-aided simulation of cold-formed members with regard to local stability are complicated and demand specialised or unavailable knowledge from the designer (e.g. measured or assumed imperfections, implementation of residual stresses and modifications to mechanical properties of steel at heavily deformed areas);
- Basing on our professional experience and familiarity with the industrial environment, we can state that the

aforementioned methods are not very popular among designers due to their excessive difficulty, low cost-effectiveness or lack of an uniform, universal procedure; as a result, they are often omitted or simplified in the process of design;
- It is necessary to develop a relatively simple method capable of providing safety and reliability of design even at cost of over-estimation and excessive safety factor;
- Numerical approach consisting of LBA and GNMA analyses with perfect geometry and no initial stresses managed to estimate the real ultimate load capacity, however the achieved results were too optimistic and should be treated with a reasonable safety factor; the factor is best applied to the yield stress value in GMNA analysis and even a 15% reduction might give reasonable results;
- By no means should thin-walled structures be computed using a single solid element per wall thickness; regretfully it is not uncommon among designers to do so, because solid geometrical models of a given structure are often readily available in the design office; these models should be transformed to shell models because of the well-known issues with volumetric locking and excessive bending stiffness;
- We suggest that the γ_{m0} safety factor applicable to the class 3 and 4 cross-sections in Eurocode 3 should not be considered 1.0 in case of high-strength steel, since at the present form it puts the designed structures on the verge of safety; this statement is in line with that of other researchers [17]; we suggest that the plastic yield stress value should be reduced by a factor of at least 0.85;
- Elastic–perfect plastic material model produced safer (lower) ultimate load values than the real experimental strain-stress relation despite the possibly dangerous over-estimation of Young's modulus near the yield stress value;
- The study was limited by not including residual stresses and geometrical imperfections in the numerical computations; it was howover the aim of the study to evaluate methods lacking in these features to reflect simple design conditions.

ACKNOWLEDGEMENTS

The experimental research was carried out with support from and in cooperation with the RCV manufacturing company ZOELLER TECH Sp. z o.o. The FEM calculations presented in the paper were carried out at the TASK Academic Computer Center in Gdansk, Poland.

REFERENCES

1. Abambres M, Quach W-M. Residual stresses in steel members: a review of available analytical expressions. International Journal of Structural Integrity. Emerald; 2016 Feb;7(1):70–94.

2. Bielski P, Wysocki O, Czyżewicz J. Failure of cold-formed beam: How does residual stress affect stability? Shell Structures: Theory and Applications. 2017;4:529-32. CRC Press / Balkema.

3. Cold-Formed Steel Design Manual, American Iron and Steel Institute, 2013

4. Crisfield MA. A fast incremental/iterative solution procedure that handles "snap-through." Computational Methods in Nonlinear Structural and Solid Mechanics. Elsevier; 1981;55–62.

5. Eurocode 3: Design of Steel Structures, Parts 1-1, 1-3 and 1-5, European Comittee for Standarization, 2004.

6. Ingvarsson L. Cold-forming residual stresses effect on buckling. University of Missouri-Rolla. 1975.

7. Laím L, Rodrigues JPC, Silva LS da. Experimental and numerical analysis on the structural behaviour of cold-formed steel beams. Thin-Walled Structures. Elsevier BV; 2013 Nov;72:1–13.

8. Lu Y, Li W, Zhou T, Wu H. Novel local buckling formulae for cold-formed C-section columns considering end condition effect. Thin-Walled Structures. Elsevier BV; 2017 Jul;116:265–76.

9. Niklas K. Strength analysis of a large-size supporting structure for an offshore wind turbine. Polish Maritime Research. 2017 Apr 25;24(s1):156-65.

10. Olovsson L, Simonsson K, Unosson M. Shear locking reduction in eight-noded tri-linear solid finite elements. Computers & structures. 2006 Feb 1;84(7):476-84.

11. Quach WM. Residual stresses in cold-formed steel sections and their effect on column behaviour (Doctoral dissertation, The Hong Kong Polytechnic University). 2005.

12. Quach WM, Qiu P. Strength and ductility of corner materials in cold-formed stainless steel sections. Thin-Walled Structures. Elsevier BV; 2014 Oct;83:28–42.

13. Schafer B., Peköz T. Computational modeling of cold-formed steel: characterizing geometric imperfections and residual stresses. Journal of Constructional Steel Research. Elsevier BV; 1998 Sep;47(3):193–210.

14. Schafer BW, Pekoz T. Direct strength prediction of cold-formed steel members using numerical elastic buckling solutions. 14th International Specialty Conference on Cold-Formed Steel Structures. 1998;69-76.

15. Szymczak C, Kujawa M. On local buckling of cold-formed channel members. Thin-Walled Structures. Elsevier BV; 2016 Sep;106:93–101.

16. Winful D, Cashell KA, Afshan S, Barnes AM, Pargeter RJ. Elevated temperature material behaviour of high-strength steel. Proceedings of the Institution of Civil Engineers - Structures and Buildings. Thomas Telford Ltd.; 2017 Nov;170(11):777–87.

17. Wang J, Afshan S, Schillo N, Theofanous M, Feldmann M, Gardner L. Material properties and compressive local buckling response of high strength steel square and rectangular hollow sections. Engineering Structures. Elsevier BV; 2017 Jan;130:297–315.

18. Weng CC, Pekoz T. Residual Stresses in Cold-Formed Steel Members. Journal of Structural Engineering. American Society of Civil Engineers (ASCE); 1990 Jun;116(6):1611–25.

19. Woloszyk K, Kahsin M, Garbatov Y. Numerical assessment of ultimate strength of severe corroded stiffened plates. Engineering Structures. Elsevier BV; 2018 Aug;168:346–54.

20. Wong YW. Analysis of wrinkle patterns in prestressed membrane structures. PhD Thesis, University of Cambridge, Department of Engineering, August. 2000 Aug.

21. Yu C, Schafer BW. Local Buckling Tests on Cold-Formed Steel Beams. Journal of Structural Engineering. American Society of Civil Engineers (ASCE); 2003 Dec;129(12):1596–606.

22. Yu C, Schafer BW. Simulation of cold-formed steel beams in local and distortional buckling with applications to the direct strength method. Journal of Constructional Steel Research. Elsevier BV; 2007 May;63(5):581–90.

CONTACT WITH THE AUTHORS

Paweł Bielski
e-mail: pawbiels@pg.edu.pl
Gdansk University of Technology
Narutowicza 11/12
80-233 Gdansk
Poland

Leszek Samson
e-mail: lessamso@pg.edu.pl
Gdansk University of Technology
Narutowicza 11/12
80-233 Gdansk
Poland

Oskar Wysocki
e-mail: oskwys@gmail.com
Gdansk University of Technology
Narutowicza 11/12
80-233 Gdansk
Poland

Jacek Czyżewicz
e-mail: jacczyze@pg.edu.pl
Gdansk University of Technology
Narutowicza 11/12
80-233 Gdansk
Poland